IEEE Access
Multidisciplinary | Rapid Review | Open Access Journal

Received April 24, 2020, accepted May 10, 2020, date of publication May 14, 2020, date of current version May 28, 2020.

Digital Object Identifier 10.1109/ACCESS.2020.2994530

Fault-Tolerant Stability Control for Independent Four-Wheel Drive Electric Vehicle Under Actuator Fault Conditions

KIBEOM LEE[1] AND MINYOUNG LEE[2]
[1]School of Mechanical and Automobile Engineering, Halla University, Wonju 26404, South Korea
[2]Department of Smart Industrial Machine Technologies, Korea Institute of Machinery and Materials (KIMM), Daejeon 34103, South Korea

Corresponding author: Minyoung Lee (lighton@kimm.re.kr)

This work was supported by the Institute of Civil Military Technology Cooperation funded by the Defense Acquisition Program Administration and Ministry of Trade, Industry and Energy of Korean Government under Grant UM19303RD3.

ABSTRACT Various torque distribution and stability control algorithms have been studied along with the development of four-wheel drive vehicles. But, most of those algorithms focus only on performance improvement. Since the independent four-wheel drive system is based on four drive motors, faults can occur in a motor or an inverter. If a fault occurs, the vehicle stability is not guaranteed and a fatal accident can occur. In this study, the fault-tolerant stability control algorithm for remaining healthy motors is proposed. This fault-tolerant control (FTC) system contains torque distribution and stability control algorithms. For accurate control of motor allocation, driving conditions such as under/over-steering, and steering direction should be considered, as well as vehicle condition such as fault motor location and motor performance limits. The proposed FTC is evaluated with two fault conditions (e.g., front motor fault, rear motor fault) under straight acceleration and constant steering acceleration scenarios. The behavior characteristics and driving risks caused by failures of motors while driving are analyzed. Also, the FTC algorithm is accurately follow a desired path within a minimum error range that the driver can cover.

INDEX TERMS Fault-tolerant control, four-wheel drive, in-wheel motor, micro electric vehicle, stability control.

I. INTRODUCTION

Air pollution and global warming are increasing due to large masses of vehicles and large population density in mega cities. To satisfy more stringent regulations, many car manufacturers have developed technology for high fuel efficiency and green cars, e.g., hybrid vehicles, fuel cell electric vehicles, and pure electric vehicles. Because they produce less noise and pollution, electric vehicles are gaining more attention. Besides the environmental aspects, the advantages of EVs are 1) Torque generation of an electric motor is very quick and accurate; 2) Small motors allow direct drive to each wheel; and 3) Motor drive torque can be measured easily [1]. Recently, several commercialized vehicles have had independent four motor or dual motor configurations [2].

The associate editor coordinating the review of this manuscript and approving it for publication was Youqing Wang.

In-wheel systems have been developed to highlight the advantages of independent drives and space utilization. In-wheel motors are those in which all components can be mounted in the wheel, e.g., motor, brake, and suspension [3]–[5]. In-wheel motors leave lots of space for passenger convenience and safety devices because they do not need a separate motor area in the chassis [6], [7].

In order to improve the performance of independent drive motors, the in-wheel motor structure has been studied to satisfy requirements of vehicle performance. As well as miniaturization, various pole-slot structures have been proposed to facilitate the high torque density, wide speed range, and high efficiency characteristics suitable for electric vehicles as detailed by Chung *et al.* [8], Fan *et al.* [9], and Peng and Flack [10]. The wireless in-wheel motor is proposed to solve the disconnection and vibration problem detailed by Sato *et al.* [11]. A dynamic vibration absorbing structure for

vibration mitigation in wheel motors has been proposed by Qin *et al.* [12].

After studying the in-wheel motor structure, improving the control performance has been studied, especially for the problem of vibration. A control method to analyze and solve vibration problems caused by rotor position errors in electric wheel motors was proposed by Mao *et al.* [13]. The neural network inverse and state feedback control method was proposed for robust pole placement by Li *et al.* [14]. These studies have solved the structural and control problems of the in-wheel systems.

Study was conducted to increase the vehicle dynamics performance using In-wheel systems. Because the four motors are controlled independently, a torque distribution algorithm is needed to distribute the torque according to the speed and steering angle. An optimal torque distribution control strategy for improving vehicle handling and stability was proposed by Li *et al.* [15]. A real-time torque distribution strategy was proposed by Wang *et al.* [16]. This strategy not only increased the dynamic performance of the vehicle but also increased the energy efficiency. A torque distribution method for the skid system was proposed by Liao *et al.* [17]. This method is able to achieve proper rotational performance using only torque distribution, without engaging the steering system.

Independent four-wheel drive systems allow easy control of yaw stability because each wheel can directly generate independent braking and acceleration and accurately measure torque. A new electronic stability control algorithm was proposed by Zhai *et al.* using the driving and braking forces of each wheel motor [18]. Enhancing the vehicle dynamic performance and turning performance in sliding condition using direct yaw moment control was proposed by Kobayashi *et al.* [19], Guo *et al.* [20], and Hu *et al.* [21]. MPC-based yaw stability control using active front steering and motor torque distribution was proposed by Ren *et al.* [22]. Most studies, however, have focused on improving the performance of independent four-wheel drives. There have been limited studies on problems that can be caused by faulty independent drives.

In conventional vehicles with internal combustion engines, the vehicle cannot drive when the engine fails. However, independent four-wheel drive vehicles have four motors as driving sources. If one or two motors and inverters break down, the vehicle can drive under limited conditions. However, such failure conditions cause instability problems, and so a system that can mitigate these problems is essential. Fault scenarios that can occur during driving are shown in Fig. 1. The red dashed line is the expected vehicle driving path without fault-tolerant control. Such a path can cause a collision with nearby vehicles or vehicles in the opposite lane. The blue line is the expected vehicle driving path with fault-tolerant control. Collision risk can be avoided by using a torque distribution and stability control algorithm controlled by the remaining operating motors.

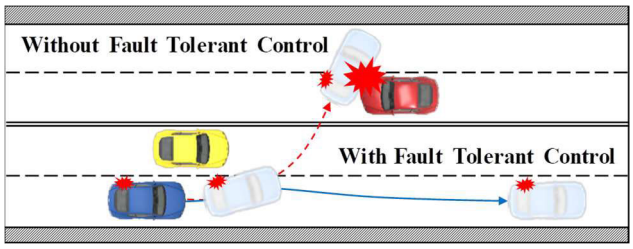

FIGURE 1. Independent four-wheel drive vehicle fault scenario.

Various fault tolerant control algorithms have been studied to solve safety problems. Anti-slip control for fault-tolerant traction control was proposed by Hu *et al.* [23]. However, this study focuses on longitudinal control; the yaw stability is not considered. Sliding mode control for in-wheel motors and electro-mechanical brakes was proposed by Kim *et al.* [24]. In that algorithm, only the brakes were used to yaw moment control. After that, a study of fault-tolerant stability control considering motor acceleration was conducted. Fault diagnosis and redistributing of torque to healthy wheels was studied by Wang *et al.* [25], [26]. A robust gain-scheduling algorithm was proposed by Zhang *et al.* [27]. However, these studies focused on control of the yaw moments and the stability. These algorithms do not consider control wheel allocation under over/under-steering, or steering direction conditions. Also, these algorithms do not consider the performance limits of the drive motor. It is not possible to cover all situations that occur while driving a vehicle.

In this study, the motor short-circuit condition is targeted because it generates drag and disturbance torques and has important effects on vehicle stability. The behavior of the vehicle depends on the location of the failed motor (e.g., front, rear), and appropriate response is required depending on the type of fault mode. Also, consideration of the motor performance limitations is essential to control the stability. The proposed fault-tolerant control (FTC) algorithm is constructed considering the motor performance limits and an electronic stability control (ESC) algorithm using three wheels. The algorithm's aim is to keep overall drift during 100 meters of driving to under one meter, so as to prevent invasion of other lanes and guarantee steering control ability to the driver. This can increase the controllability when a motor fault occurs during driving. So, vehicle accidents caused by motor faults can be reduced. The main contribution of this paper is: (1) The fault modes of independent four-wheel drive are analyzed. The FTC algorithm can be designed considering all possible fault conditions, not one small condition. (2) The vehicle dynamics for each fault mode is analyzed. From the viewpoint of vehicle dynamics, the severity of the one motor fault is identified, the control wheel is allocated with the best efficiency. (3) A fault-tolerant control algorithm with electronic stability control is designed considering the motor fault mode. Stability control can be performed with the healthy wheels, excluding the faulty ones. (4) Performance evaluation

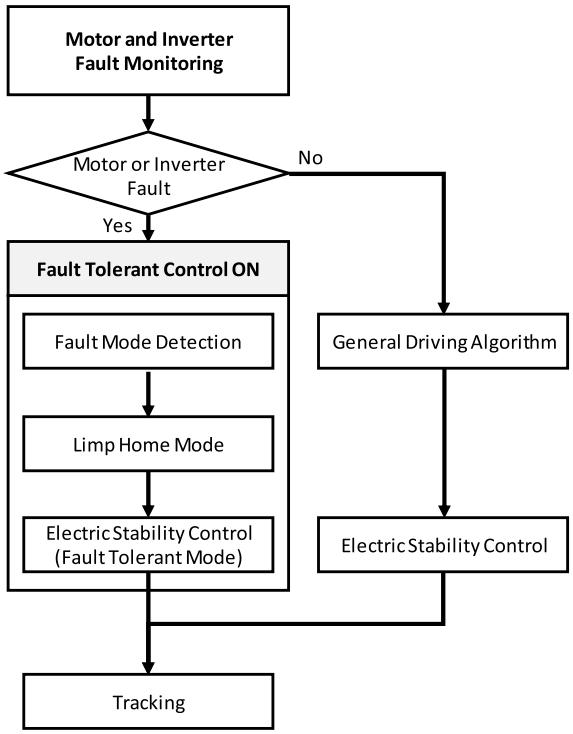

FIGURE 2. Flow chart of Fault-tolerant control (FTC).

is performed through scenario simulation. Through the simulation, the stability improvement through the algorithm is verified.

The remainder of this paper is organized as follows: In Section II, an architecture for fault-tolerant control is proposed. Vehicle modeling for the algorithm is carried out in section III. In section IV, the fault-tolerant control system design is proposed. In section V, evaluation of the performance of the designed fault-tolerant control algorithm is carried out with scenario simulation. Finally, Section VI provides concluding remarks.

II. ARCHITECTURE OF FAULT TOLERANT CONTROL AND FAULT MODE

A. FAULT-TOLERANT CONTROL SYSTEM

A flow chart of the fault-tolerant control system is shown in Fig. 3. The monitoring system always monitors the status of the motor and inverter for checking faults. In there is no fault condition, the general driving algorithm and general ESC distribute the torque and control the stability of the vehicle. If a fault occurs in a motor or inverter, the FTC is activated.

The FTC consists of a limp home mode (LHM) module and an electronic stability control (ESC) module. LHM is a driving mode that minimizes unbalanced moment influence during periods of decreased total vehicle torque due to a single motor fault. ESC is a vehicle stability control unit using the desired yaw rate. In the fault mode, considering that there is a faulty motor, vehicle stability is controlled only by the other motors.

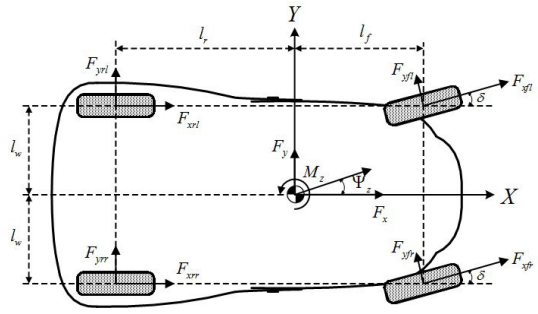

FIGURE 3. Vehicle body model schematic diagram.

The desired yaw rate is calculated according to the steering angle and the vehicle velocity. The desired yaw rate is compared with the measured yaw rate and each wheel torque is redistributed to reduce the gap between desired yaw rate and measured yaw rate. In a conventional vehicle, torque distribution is used for independent braking. However, independent four-wheel drive systems can control each wheel motor separately, and so it is easy to control the stability by increasing or decreasing the torque.

B. TYPICAL FAULT MODE IN MOTOR

The results of motor failure modes and effects analysis (FMEA) are shown in Table 1 [28]. The highest risk priority number is that of high magnetization, but this is easy to detect and the motor can be controlled to subdue the issue. So, in this study, the proposed algorithm is focused on short circuits and open circuits faults. When open-circuit faults occur, a high torque ripple and loss of torque appear; disturbance torque does not appear. However, with short-circuit faults, large circulating currents occur that generate large disturbance torques. Generally, short-circuits are caused by winding, power device, or power supply capacitor failure. Disturbance torque caused by a short circuit makes the vehicle unstable. So, detection of short circuits and transforming them to open circuits are important.

TABLE 1. Results of motor failure modes and effects analysis.

Failure Mode	Severity Rating (S)	Occurrence Rating (O)	Detection Rating (D)	Risk Priority Number (S x O x D)
Too High Magnetization - Lost current in field weakening range	8	5	6	240
Short Circuit	8	3	6	114
Open Circuit	8	4	3	96
High Impedance	4	2	8	64
Rotor Body - Magnets Fall Off	8	1	8	64
Too Low Magnetization - Demagnetized	6	2	2	24
Shaft -Overload (torque)	8	1	3	24

C. FAULT DETECTION AND FAULT-TOLERANT INVERTERS

Fault detection and fault diagnosis algorithms have been studied by Si *et al.* [29], Wang *et al.* [30], and Zhou *et al.* [31]. Also, Motor fault detection and fault-tolerant control for motors have been studied by Jack *et al.* [32] and Bianchi *et al.* [33]. The test platform used in this study is equipped with a permanent magnet synchronous motor (PMSM), and fault detection and fault-tolerant control have been studied by Rosero *et al.* [34], Wallmark *et al.* [35], and Jeong *et al.* [36]. A short-circuit fault detection method using quadratic time-frequency (TF) analysis for PMSM was proposed by Rosero *et al*. [34]. The quadratic TF algorithm, verified by simulation and experiment, was used for PMSM fault detection. A fault-tolerant inverter configuration was proposed by Wallmark *et al.* [35]. The fault-tolerant inverter for PMSM drives uses extra switches (e.g., BJT, FET) to isolate shorted phase incidence. After isolation, post fault operation can be possible. In this research, using the Y-connection method, the extra switches are connected to a neutral point of the PMSM. The motor fault tolerant system is mounted in each motor; this study focuses on FTC at the vehicle dynamics level.

III. MODELING OF INDEPENDENT DRIVE VEHICLES

A. VEHICLE MODEL

A full car model with longitudinal, lateral, and yaw motions, excluding roll and pitch motions, is used for vehicle control, as shown in Fig. 3. [37].

The vehicle's x-axis force, y-axis force, and z-axis moment are calculated as Eqs. (1)-(3).

$$\begin{aligned} \mathrm{F_x} &= m\ddot{x} = \left(F_{xfl} + F_{xfr}\right)\cos(\delta) \\ &\quad - \left(F_{yfl} + F_{yfr}\right)\sin(\delta) + \mathrm{F_{xrl}} + F_{xrr} \end{aligned} \tag{1}$$

$$\begin{aligned} \mathrm{F_y} &= m\ddot{y} = \left(F_{yfl} + F_{yfr}\right)\cos(\delta) \\ &\quad + \left(F_{xfl} + F_{yfr}\right)\sin(\delta) + F_{yrl} + F_{yrr} \end{aligned} \tag{2}$$

$$\begin{aligned} \mathrm{M_z} &= I_z\ddot{\Psi} = l_f\left(F_{xfl} + F_{xfr}\right)\sin(\delta) \\ &\quad + l_f\left(F_{yfl} + F_{yfr}\right)\cos(\delta) + \frac{l_w}{2}\left(F_{xfr} - F_{xfl}\right)\cos(\delta) \\ &\quad + \frac{l_w}{2}\left(F_{yfl} - F_{yfr}\right)\sin(\delta) - l_r\left(F_{yrl} + F_{yrr}\right) \\ &\quad + \frac{l_w}{2}(F_{xrr} - F_{xrl}) \end{aligned} \tag{3}$$

where $\mathrm{F_x}$ and $\mathrm{F_y}$ are the longitudinal and lateral forces respectively, $\mathrm{I_z}$ is the z-axis moment of inertia, $\mathrm{l_r}$ is the length from the center of gravity to the rear wheel center, $\mathrm{l_f}$ is the length from the center of gravity to the front wheel center, $\mathrm{l_w}$ is half of the wheel track, m is the mass of vehicle, $\mathrm{M_z}$ is the moment of the z-axis, Ψ is the yaw angle, and δ is the steering angle. The subscript *rl* is the rear left tire, *rr* is the rear right tire, *fl* is the front left tire, and *fr* is the front right tire.

B. TIRE MODEL

The magic formula tire force model proposed by Pacejka is used for the simulation [38]. It is incorporated into CarSim®. In these models, a combined slip situation is modeled from a physical viewpoint. The results from the model match well with the experimental data for cases of pure lateral or pure longitudinal force generation [38], [39]. The general form of the formula is described in Eqs. (4)-(6).

$$y = D\sin\left[Carctan\left\{Bx - E\left(\mathrm{Bx\text{-}arctanBx}\right)\right\}\right] \tag{4}$$

$$Y(X) = y(x) + S_y \tag{5}$$

$$x = X + S_h \tag{6}$$

where Y is the output variable F_x and F_y, X is the input variable slip angle or slip ratio; I is the stiffness factor, C is the shape factor, D is the peak value, E is the curvature factor, S_h is the horizontal shift, and S_v is the vertical shift.

This tire model can be represented on the x-y axis using the friction limit, as shown in Fig. 4. The simplified friction limit equation is shown in Eq. (7). Due to the friction limit, the combined longitudinal and lateral acceleration that the tire can generate is limited. This means that the lateral force can be reduced and the moment can change when longitudinal force is generated to control stability. Therefore, when controlling the vehicle stability in ESC, it is necessary to select the wheel motors that can be efficiently controlled according to whether the situation involves over-steering or under-steering.

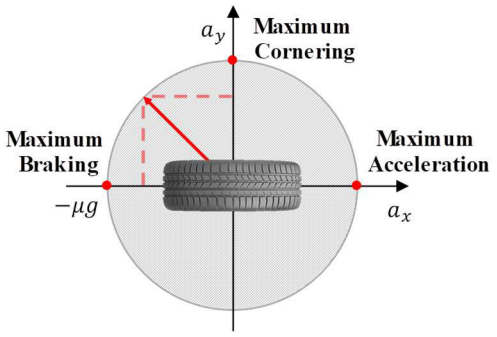

FIGURE 4. Tire friction limit schematic diagram.

$$(\mu g)^2 = a_x^2 + a_y^2 \tag{7}$$

where $\mathrm{a_x}$ and $\mathrm{a_y}$ are the longitudinal acceleration and the lateral acceleration, respectively, μ is the friction coefficient, and g is the gravitational acceleration.

C. DRIVE WHEEL MOTOR MODEL

A torque speed curves for the PMSM drive motor is shown in Fig. 5. The peak torque is 64.5Nm and maximum speed is 600RPM. Depending on the characteristics of the motor, the maximum torque is generated at low speeds; the generated torque decreases as the speed increases at high speed (above 250RPM). Since the torque limit depends on the speed, the torque distribution algorithm is necessary to consider the torque limit at each speed.

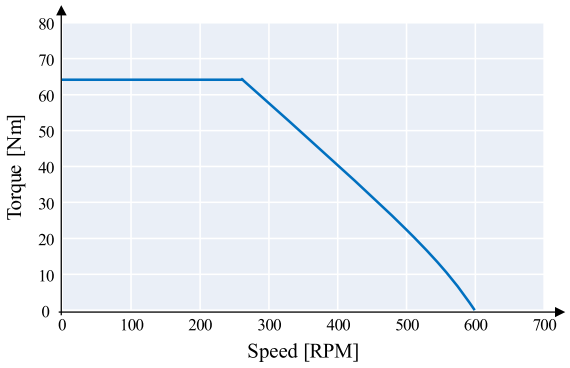

FIGURE 5. Drive motor torque speed curve.

IV. FAULT-TOLERANT CONTROL SYSTEM DESIGN

The proposed fault-tolerant control architecture is shown in Fig. 6. When a motor fault occurs, the limp home mode and electric stability control algorithm operate simultaneously to ensure yaw stability. In a fault situation, the electronic stability control (ESC) must operate on all normal drive wheel motors except for the broken wheel motor. This section introduces the limp home mode (LHM), used to control the yaw moment balance at high level phase, and the fault-tolerant electronic stability control system (FT-ESC), used to control the yaw stability so that vehicle can operate in fault conditions at low level phase.

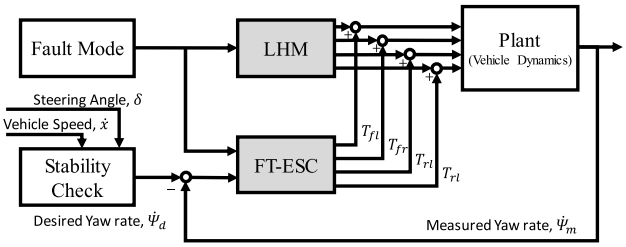

FIGURE 6. Fault-tolerant control (FTC) schematic diagram.

A. LIMP HOME MODE (LHM)

Limp home mode is used to adjust the yaw moment of the vehicle, and offers a high level of control. LHM is applied after fault detection and changes the drag force to zero. The faulty motor, after fault-tolerant action, does not generate disturbance torque; however, it cannot generate drive torque either. If one motor fails to generate torque, moment imbalance of the vehicle occurs and drift becomes large. To prevent drifting problems when one motor fails, the other motor on the same side must enhance the torque to balance the yaw moment. This can stabilize the yaw moment. However, if the other motor reaches its torque limit, the opposite side motor must reduce its torque.

An example of LHM is shown in Fig. 7. If the front left motor fails and generates zero drive torque, the rear left motor must produce twice the required torque, as shown in Fig. 7(a). However, if the rear left motor reaches its torque limit, the rear

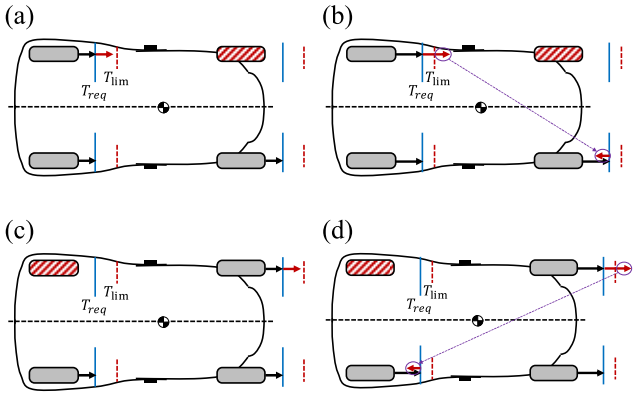

FIGURE 7. Limp home mode (LHM) scheme. (a) Front left (FL) fault mode for case 1. (b) Front left (FL) fault mode for case 2. (c) Rear left (RL) fault mode for case 1. (d) Rear left (RL) fault mode for case 2.

right motor must reduce by excess torque to match moment stability, as shown in Fig. 7(b). This control method decreases the acceleration and speed performance of the vehicle, but can increase safety.

An example in which there is a fault in the front left wheel motor is shown in Eqs. (8) and (9). The equation of torque distribution can be expressed for two cases. In the first case, the summation of requested torque is lower than the motor torque limit. In the second case, the summation of requested torque is over the motor torque limit.

Case 1: $T_{fl_{req}} + T_{rl_{req}} \leq T_{lim}$

$$\begin{cases} T_{fl} = 0\,(Fault) \\ T_{fr} = T_{fr_{req}} \\ T_{rl} = T_{rl_{req}} + T_{fl_{req}} \\ T_{rr} = T_{rr_{req}} \end{cases} \tag{8}$$

Case 2: $T_{fl_{req}} + T_{rl_{req}} > T_{lim}$

$$\begin{cases} T_{fl} = 0(Fault) \\ T_{fr} = T_{fr_{req}} - (T_{fl_{req}} + T_{rl_{req}} - T_{lim}) \\ T_{rl} = T_{lim} \\ T_{rr} = T_{rr_{req}} \end{cases} \tag{9}$$

where T is the wheel motor torque; the subscript rl is the rear left tire, rr is the rear right tire, fl is the front left tire, fr is the front right tire, lim is the torque limitation, and req is the required torque.

An example in which there is a fault in the rear left wheel motor is expressed in Eqs. (10) and (11). As before, there are two cases, one in which the requested motor torque is lower than the motor torque limit and one in which the requested motor torque exceeds the torque limit.

Case 1: $T_{fl_{req}} + T_{rl_{req}} \leq T_{lim}$

$$\begin{cases} T_{fl} = T_{fl_{req}} + T_{rl_{req}} \\ T_{fr} = T_{fr_{req}} \\ T_{rl} = 0\,(Fault) \\ T_{rr} = T_{rr_{req}} \end{cases} \tag{10}$$

Case 2: $T_{xfl_{req}} + T_{xrl_{req}} > T_{lim}$

$$\begin{cases} T_{fl} = T_{lim} \\ T_{fr} = T_{fr_{req}} \\ T_{rl} = 0(Fault) \\ T_{rr} = T_{rr_{req}} - (T_{fl_{req}} + T_{rl_{req}} - T_{lim}) \end{cases} \tag{11}$$

B. FAULT-TOLERANT ELECTRONIC STABILITY CONTROL (FT-ESC)

The ESC maintains the moment stability by generating independent wheel motor torques. However, under a motor fault condition, a different ESC algorithm is needed because the faulty wheel motor cannot generate correct torque. A different control algorithm is needed for each faulty wheel motor location, for cases of over-steering case and under-steering, and for steering direction. The detailed control algorithm is described as follows.

The torque distribution algorithm for a front left motor fault condition is shown in Fig. 8. In this case, front left motor cannot generate drive torque and the rear left motor generates the total required torque, that is, the sum of torque of the front left and rear left motors, as in limp home mode.

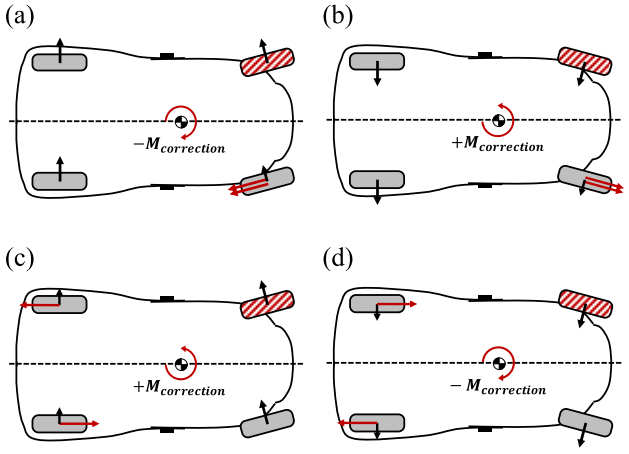

FIGURE 8. Torque distribution method for front left (FL) motor fault. (a) Over-steering case with left steering, (b) Over-steering case with right steering, (c) Under-steering case with left steering, (d) Under-steering case with right steering.

Over-steering cases with left and right steering are shown in Fig. 8(a) and (b), respectively. Negative moment is needed when over-steering occurs during left steering, as shown in Fig. 8(a). In the case of the rear left and right motor, the lateral force decreases when accelerating and braking force are generated based on the tire friction limit. This condition simultaneously generates positive moment due to lateral forces and negative moment due to accelerating and braking forces, reducing the stability control efficiency. Therefore, negative moment should be only generated through the front right motor.

Positive moment is needed when over-steering occurs during right steering, as shown in Fig. 8(b). When the acceleration force is generated on the rear left and right motor, the lateral force is reduced and negative moment is generated. Therefore, positive moment should be only generated through the front right motor.

Under-steering cases with left steering and right steering are shown in Fig. 8(c) and (d), respectively. Positive moment is needed when under-steering occurs during left steering, as shown in Fig. 8(c). When acceleration force is generated by the front right motor, the lateral force is reduced and negative moment is generated. Therefore, the braking force of the rear left and the acceleration force of the rear right motor should be generated at the same time. In this case, moment force can only be generated when there is no change of the longitudinal acceleration.

Negative moment is needed when under-steering occurs during right steering, as shown in Fig. 8(d). In the case of the front right motor, the lateral force decreases when braking force is generated. This condition simultaneously generates negative moment due to lateral force and positive moment due to braking force, reducing the stability control efficiency. Therefore, acceleration force of the rear left and braking force of the front right motors should be generated at the same time.

The torque distribution algorithm for a rear left motor fault condition is shown in Fig. 9. In this condition, rear left motor cannot generate drive torque and the front left motor generates the required torque of the front left plus rear left motor, as in limp home mode.

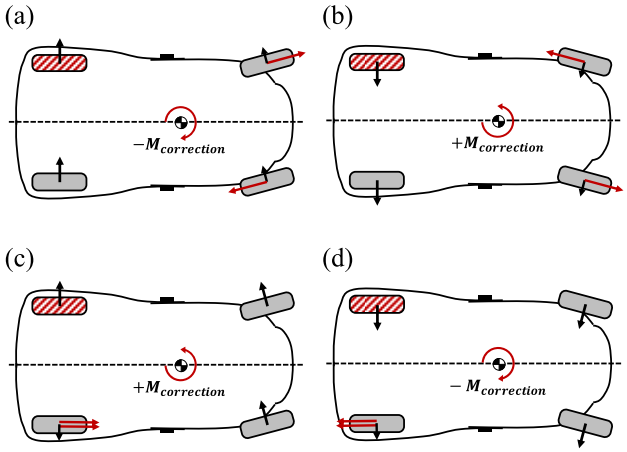

FIGURE 9. Torque distribution method for rear left (RL) motor fault. (a) Over-steering case with left steering, (b) Over- steering case with right steering, (c) Under- steering case with left steering, (d) Under- steering case with right steering.

As in the front left motor fault case, the control motor is determined by the over-steering case, under-steering case, and steering directions. In the over-steering case with left steering, the moment is controlled by the front left and right motors simultaneously, as shown in Fig. 9(a). In the over-steering case with right steering, the front left and the front right motors are controlled simultaneously, as shown in Fig. 9(b). In the under-steering case with left steering, the rear right motor is controlled, as shown in Fig. 9(c).

In the under-steering case with right steering, the moment is controlled by the rear right motor, as shown in Fig. 9(d).

According to the fault mode, the electronic stability control algorithm is used to determine which wheel motor should be controlled in over-steering and under- steering situations. In each condition, control wheel allocation summary is shown in Table. 2.

TABLE 2. Control wheel allocation strategy for the over-steering and under-steering cases.

Driving Condition		Control Wheel Allocation			
		Front left (FL)	Front right (FR)	Rear left (FL)	Rear right (RR)
Over-steering Case	Left Steering	Fault	--	Req	Req
		+	-	Fault	Req
	Right Steering	Fault	++	Req	Req
		-	+	Fault	Req
Under-steering Case	Left Steering	Fault	Req	-	+
		Req	Req	Fault	++
	Right Steering	Fault	Req	+	-
		Req	Req	Fault	--

The torque generated for each wheel motor is determined by the difference between the desired yaw rate and the measured yaw rate, as shown in Fig. 6. The desired yaw-rate is calculated using Eq. (12). In this study, the P controller is used for feedback. The used P gain is 2.7 in this vehicle platform case. The control gain should be tuned according to vehicle specifications such as vehicle mass and cornering stiffness. When the allocated control wheel is one, the entire required torque is generated, and when it is two, the required torque is distributed in half.

$$\dot{\Psi}_{\text{des}} = \frac{\dot{x}}{R} = \frac{\dot{x}}{(l_f + l_r) + \frac{m\dot{x}^2(l_r C_{\alpha r} - l_f C_{\alpha f})}{2C_{\alpha f} C_{\alpha r}(l_f + l_r)}}\delta \tag{12}$$

V. PERFORMANCE EVALUATION WITH SIMULATION

The proposed fault-tolerant control algorithm is verified by CarSim® and Matlab/Simulink® simulation. Dynamic simulation is used to analyze changes in vehicle motion, speed, and yaw rate under motor fault conditions. The performance of this algorithm is compared with that of the algorithm without FTC. The simulation is conducted for two scenarios and four cases.

A. SIMULATION PLATFORM

A micro electric vehicle (MEV) equipped with in-wheel system is used as the simulation platform. The MEV is an electric vehicle driven by four independent motors. In the previous study, the four-wheel drive algorithm for the platform was verified [40]. Since the fault situation cannot be tested as a real vehicle, simulation evaluation is performed based on the verified vehicle model. The detailed specifications are shown in Table 3.

TABLE 3. Test vehicle platform parameters.

		Unit	Specification
Length	Overall (L x W x H)	[m]	2.82 x 1.71 x 1.66
	Folded (L x W x H)	[m]	1.65 x 1.71 x 1.83
	Wheelbase	[m]	2.10
	Wheel-track	[m]	1.50
Center of Gravity	CG to Front Wheel	[m]	1.00
	CG to Rear Wheel	[m]	1.10
	CG Height	[m]	0.430
Weight	Curb Weight (battery excluded)	[kg]	450
	Gross Vehicle Weight (GVW)	[kg]	710
	Un-sprung mass	[kg]	110
In-Wheel Motor (each)	Maximum Torque	[Nm]	64.5
	Max Speed	[RPM]	600
	Wheel & Tire		
	Wheel	[inch]	13
	Tire Diameter	[m]	0.5334 (155x65R13)

B. DRIVING SCENARIOS FOR SIMULATION

The simulation is conducted under two fault conditions, one is a front left motor fault and the other is a rear left motor fault. They are compared with no-fault, motor fault vehicle without control, and motor fault with FTC conditions. The two driving scenarios used for performance evaluation are shown in Fig. 10. Straight acceleration simulation is performed to identify vehicle drift rate under motor fault condition. Constant steer acceleration simulation is performed to identify vehicle cornering ability under motor fault condition.

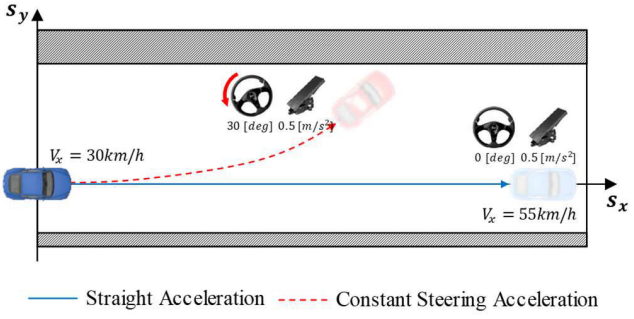

FIGURE 10. Driving scenarios for performance evaluation simulation.

1) STRAIGHT ACCELERATION DRIVING

Straight acceleration simulation is performed to identify the drift ratio of the vehicle. The simulation is performed with a constant zero steering angle. The vehicle start speed is 30km/h and vehicle accelerates at 0.5m/s^2 throttle. The road has a high friction coefficient, like that of asphalt (constant 0.85 coefficient). The two simulations are performed in these conditions: front left motor driver fault; and rear left motor driver fault.

2) CONSTANT STEERING ACCELERATION DRIVING

Constant steering acceleration simulation is performed to identify the drift ratio of the vehicle during cornering. The simulation is performed with a constant 30deg steering angle. The vehicle start speed is 30km/h and vehicle accelerates with $0.5m/s^2$ throttle. The road has a high friction coefficient, like that of asphalt (constant 0.85 coefficient). The two simulations are performed in these conditions: front left motor driver fault; and rear left motor driver fault.

C. SIMULATION RESULTS

The fault-tolerant control algorithm simulation results are compared with those of the no-fault condition and the without-FTC condition. The results are compared for two scenarios: straight acceleration scenario and constant steering acceleration driving scenario. In each scenario, the behavior and stability are discussed for cases of failure of the front and rear motors.

1) STRAIGHT ACCELERATION DRIVING

Simulation results for straight line acceleration with fault in the front left motor and in rear left motor are shown in Fig. 11 and Fig. 12. This simulation uses constant zero steering; as there is no disturbance, the vehicle should go straight.

The vehicle driving trajectories are shown in Fig. 11(a). Vehicle with a front left motor fault without FTC drifted almost 18m during 240m of driving. However, the vehicle motion under fault of the front left motor with FTC drifted just 2m during the same 240m of driving. The vehicle speed is shown in Fig. 11(b). Both fault modes have lower acceleration than that of the no-fault condition. At lower speeds, the FTC algorithm generates higher acceleration than does the system without FTC algorithm, but the acceleration decreases over time. This is because a spare motor generates additional torque to compensate for the vehicle acceleration at low speeds. However, when the requested torque exceeds the motor torque limit at high speeds, the LHM reduces the performance of the spare motor to ensure vehicle stability. The desired yaw rate is shown in Fig. 11(c). In this situation, the desired yaw rate is zero. The FTC algorithm shows yaw rates close to zero; however, without the FTC algorithm there is a range of yaw rates. Each drive motor torque is shown in Fig. 11(d). The rear left motor generates additional torque to compensate for the front left motor fault, and the front right torque is reduced to balance the yaw of the vehicle.

The same trend is seen for the rear left motor fault condition, as shown in Fig. 12. Vehicle motion with rear left motor fault without FTC algorithm drifted almost 10m during 240m of driving. Vehicle motion under fault of rear left motor with FTC algorithm drifted just 1m during the same 240m of driving, as shown in Fig. 12(a). As in the front left fault condition, at low speed, the FTC algorithm generates higher acceleration than the system without the FTC algorithm; FTC algorithm also generates lower acceleration when torque is

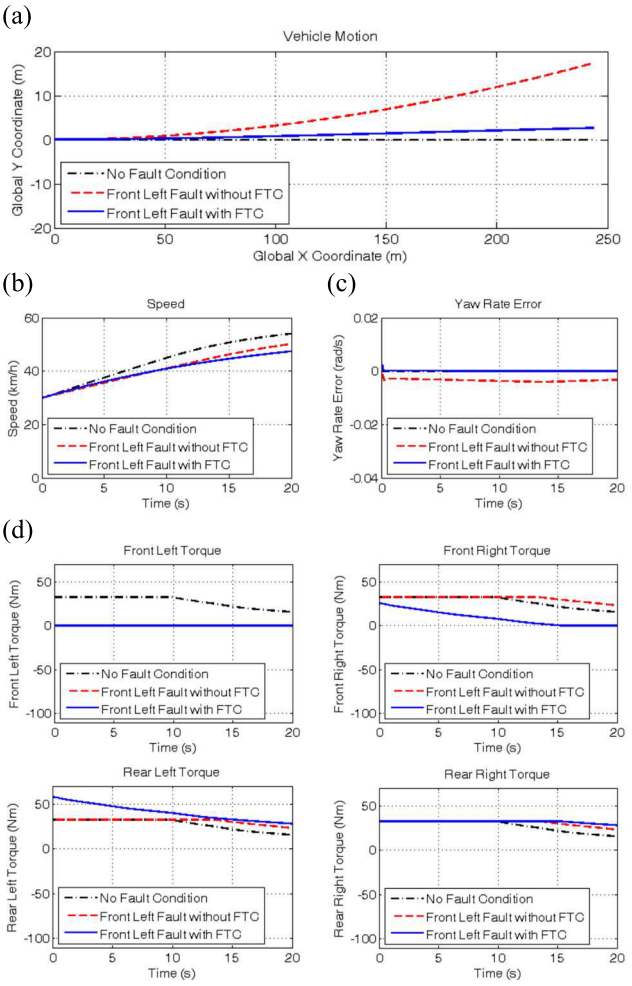

FIGURE 11. Simulation results for straight acceleration driving with fault in front left motor. (a) Vehicle motion, (b) Vehicle speed, (c) Yaw rate, (d) Torque of each wheel (Front left, Front right, Rear left, Rear right).

limited at high speed, as shown in Fig. 12(b). The front left motor generates additional torque to compensate for the rear left motor fault, and the rear right motor torque is reduced to control the yaw balance of the vehicle, as shown in Fig. 12(d).

Comparisons of the maximum offsets of each case, with 240m driving, are shown in Fig. 13. The FTC algorithm improved the front left fault by 88.9% and the rear left fault by 90.0%. This experiment shows that the severity of drifting is larger with a front motor fault than with a rear motor fault.

2) CONSTANT STEERING ACCELERATION DRIVING

Simulation results for constant steering acceleration simulations with fault in front left motor and rear left motor are shown in Fig. 14 and Fig. 15.

The vehicle driving trajectories are shown in Fig. 14(a). Vehicle with front left motor fault without FTC drifted almost 35m more than it would have drifted in no-fault condition during 140m of driving. However, the vehicle motion under fault of the front left motor with FTC drifted just 15m more than it would have drifted in no-fault condition

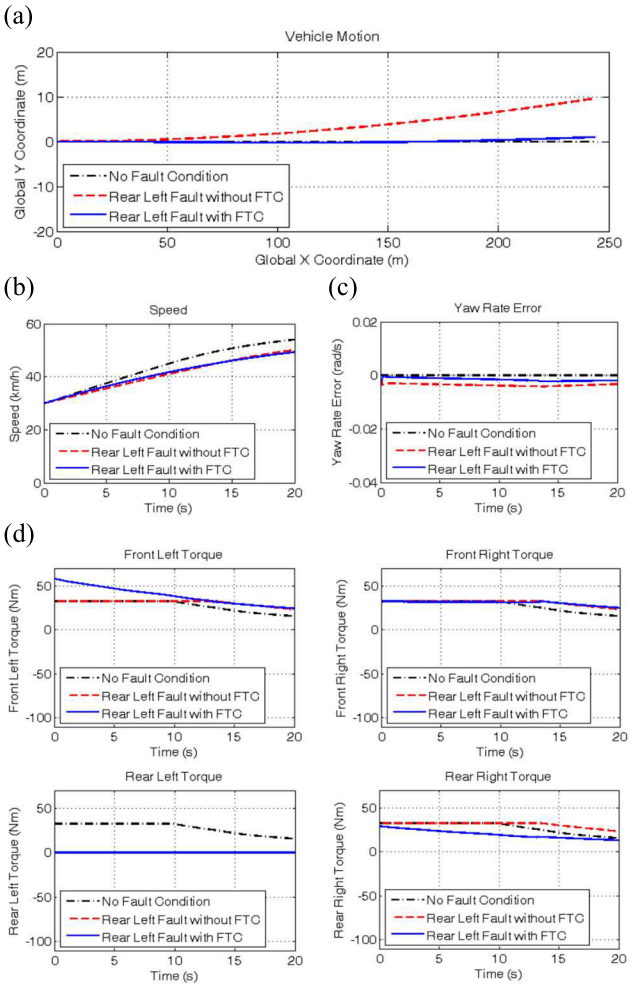

FIGURE 12. Simulation results for straight acceleration driving with fault in rear left motor. (a) Vehicle motion, (b) Vehicle speed, (c) Yaw rate, (d) The torque of each wheel (Front left, Front right, Rear left, Rear right).

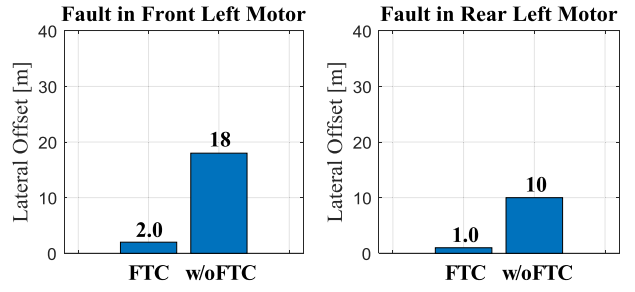

FIGURE 13. Maximum lateral offset comparison for cases with FTC algorithm and without FTC algorithm during straight acceleration driving scenario.

during the same 140m of driving. The vehicle speed is shown in Fig. 14(b). As with the straight acceleration scenario, both fault modes have lower acceleration than that of the no-fault condition. At lower speeds, the FTC algorithm generates higher acceleration than the system without FTC algorithm, but the acceleration decreases over time. The desired yaw rate

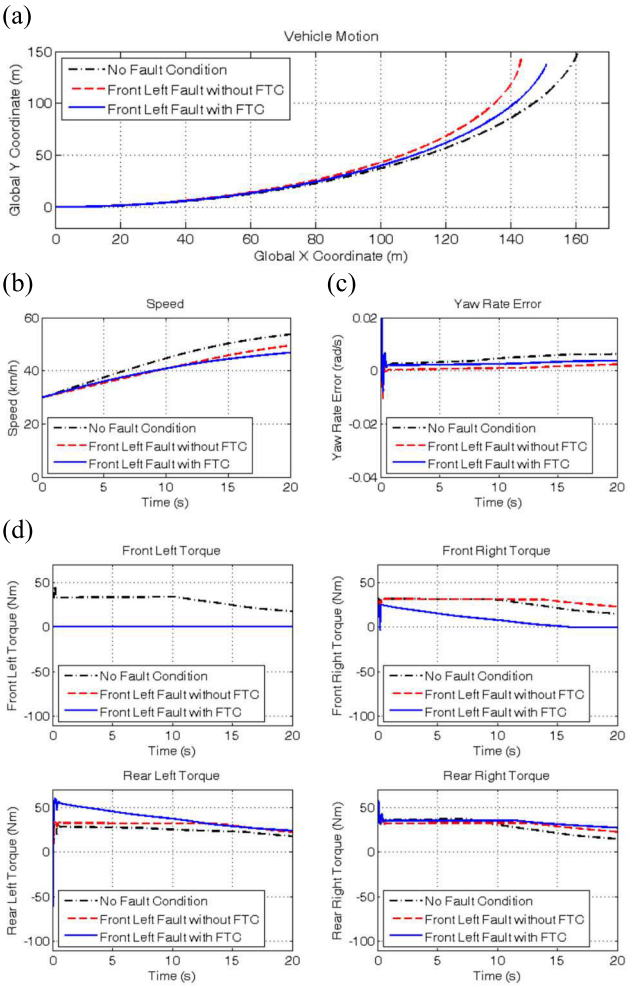

FIGURE 14. Simulation results for constant steering acceleration driving with fault in front left motor. (a) Vehicle motion, (b) Vehicle speed, (c) Yaw rate, (d) Torque of each wheel (Front left, Front right, Rear left, Rear right).

is shown in Fig. 14(c). Because the speed of the vehicle is different, an absolute yaw rate comparison for each algorithm is difficult. However, the moment a fault occurs, the yaw rate vibration of the vehicle without FTC is larger than that of the vehicle with FTC. Each motor drive torque is shown in Fig. 14(d). The rear left motor generates additional torque to compensate for the front left motor fault, and the front right torque is reduced to control the vehicle yaw balance.

The same trend is seen for the rear left motor fault condition, as shown in Fig. 15. Vehicle with rear left motor fault without FTC algorithm drifted almost 10m during 140m of driving. The vehicle under fault of rear left motor with FTC algorithm drifted 5m during the same 140m of driving, as shown in Fig. 15(a). The vehicle speed and yaw rate show the same tendencies as in the left fault condition, as shown in Figs. 15(b) and (c). The front left motor generates additional torque to compensate for the rear left motor fault, and the rear right motor torque is reduced to control the vehicle yaw balance, as shown in Fig. 15(d).

Comparison of maximum offsets up to 140m for each case are shown in Fig. 16. The FTC algorithm improved the front

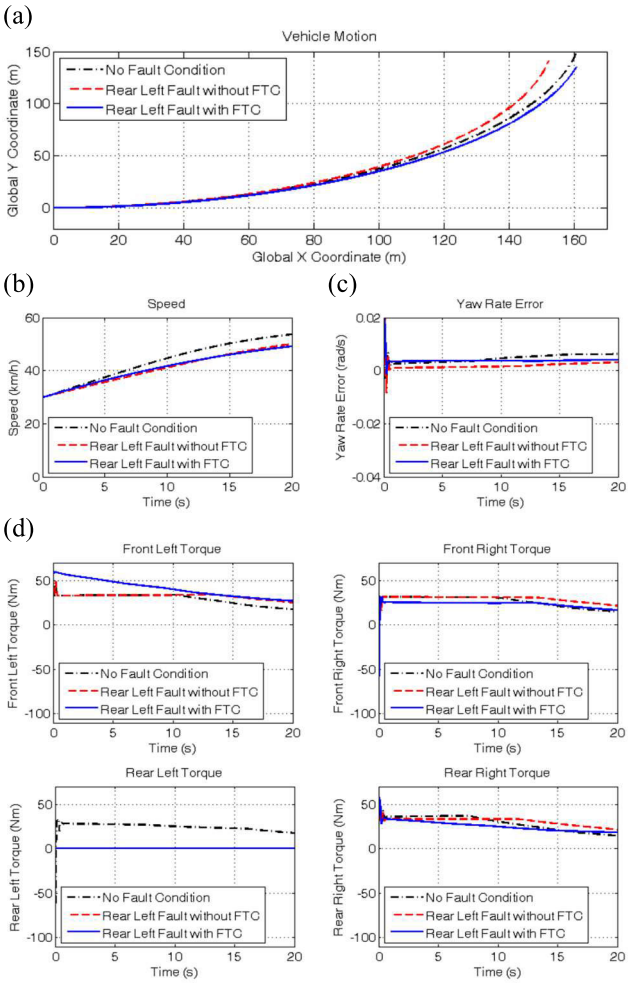

FIGURE 15. Simulation results for constant steering acceleration driving with fault in rear left motor. (a) Vehicle motion, (b) Vehicle speed, (c) Yaw rate, (d) Torque of each wheel (Front left, Front right, Rear left, Rear right).

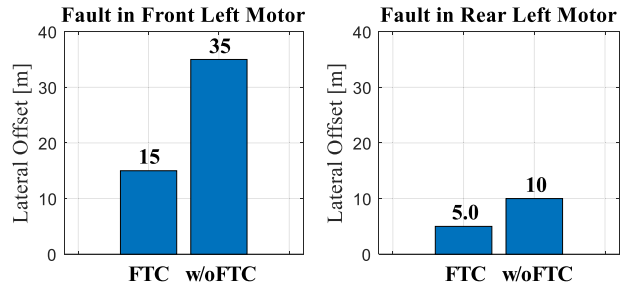

FIGURE 16. Maximum lateral offset comparison for cases with FTC algorithm and without FTC algorithm during constant steering acceleration driving scenario.

left fault by 57.1% and the rear left fault by 50.0%. Also, in a curve scenario, it can be seen that the severity of drifting is larger with a front motor fault than with a rear motor fault.

In the simulation, the effects of the FTC algorithm on vehicle yaw stability are investigated. In an independent drive vehicle, single motor failure can have a serious impact on the vehicle stability and safety. This instability can be overcome by implementing the FTC. The general ESC designed for yaw stability cannot cover motor fault conditions because it does not consider excessive yaw error or actuator motor failure. Limp home mode and FT-ESC solve this problem by considering the fault mode.

Simulations show that the effect on stability is different depending on the fault modes, e.g., front motor fault and rear motor fault. In addition, FT-ESC works properly and improves the stability in consideration of over-steering and under-steering for the various fault modes. The proposed FTC system is expected to contribute to guarantee the stability and safety of vehicle using independent four-wheel drive systems.

VI. CONCLUSION

A fault-tolerant control algorithm is proposed for a four-wheel drive in-wheel motor electric vehicle. The FTC algorithm consists of a limp home mode and an electronic stability control system for fault conditions. Through control wheel allocation considering vehicle dynamics, safe and efficient vehicle control is possible. In addition, motor performance is considered for vehicles that use low performance motors e.g., personal mobility vehicles and low speed electric vehicles. The proposed algorithm can drive the vehicle without spinning or drifting. In addition, driving with FTC is able to achieve a higher speed than driving without FTC at the one motor fault condition. The simulations show that motor faults cause serious instability and that the proposed algorithm can stably control the system. The lateral drift level is in a range that the driver can safely control through steering operations.

The proposed algorithm can increase the safety of independent drive electric vehicles with in-wheel motors. As future work, it is necessary to improve the FT-ESC by applying advanced control theories. Also, it will be interesting to consider integrating the steering control to allow stability control in fault condition.

REFERENCES

[1] Y. Hori, "Future vehicle driven by electricity and control-research on four wheel motored 'UOT Electric March II,'" *IEEE Trans. Ind. Electron.*, vol. 51, no. 5, pp. 954–962, Oct. 2004.

[2] N. Mutoh and Y. Nakano, "Dynamics of front-and-rear-wheel-independent-drive-type electric vehicles at the time of failure," *IEEE Trans. Ind. Electron.*, vol. 59, no. 3, pp. 1488–1499, Mar. 2012.

[3] S. C. Kim, W. Kim, and M. S. Kim, "Cooling performance of 25 kW in-wheel motor for electric vehicles," *Int. J. Automot. Technol.*, vol. 14, no. 4, pp. 559–567, Aug. 2013.

[4] S. Murata, "Innovation by in-wheel-motor drive unit," *Vehicle Syst. Dyn.*, vol. 50, no. 6, pp. 807–830, Jun. 2012.

[5] D. Kim, K. Shin, Y. Kim, and J. Cheon, "Integrated design of in-wheel motor system on rear wheels for small electric vehicle," *World Electr. Vehicle J.*, vol. 4, no. 3, pp. 597–602, 2010.

[6] J. Gu, M. Ouyang, D. Lu, J. Li, and L. Lu, "Energy efficiency optimization of electric vehicle driven by in-wheel motors," *Int. J. Automot. Technol.*, vol. 14, no. 5, pp. 763–772, Oct. 2013.

[7] J. Wang, Q. Wang, L. Jin, and C. Song, "Independent wheel torque control of 4WD electric vehicle for differential drive assisted steering," *Mechatronics*, vol. 21, no. 1, pp. 63–76, Feb. 2011.

[8] S.-U. Chung, S.-H. Moon, D.-J. Kim, and J.-M. Kim, "Development of a 20-Pole–24-Slot SPMSM with consequent pole rotor for in-wheel direct drive," *IEEE Trans. Ind. Electron.*, vol. 63, no. 1, pp. 302–309, Jan. 2016.

[9] Y. Fan, L. Zhang, J. Huang, and X. Han, "Design, analysis, and sensorless control of a self-decelerating permanent-magnet in-wheel motor," *IEEE Trans. Ind. Electron.*, vol. 61, no. 10, pp. 5788–5797, Oct. 2014.
[10] M.-T. Peng and T. J. Flack, "Design and analysis of an in-wheel motor with hybrid Pole–Slot combinations," *IEEE Trans. Magn.*, vol. 52, no. 6, pp. 1–8, Jun. 2016.
[11] M. Sato, G. Yamanoto, D. Gunji, T. Imura, and H. Fujimoto, "Development of wireless in-wheel motor using magnetic resonance coupling," *IEEE Trans. Power Electron.*, vol. 31, no. 7, pp. 5270–5278, Jul. 2016.
[12] Y. Qin, C. He, X. Shao, H. Du, C. Xiang, and M. Dong, "Vibration mitigation for in-wheel switched reluctance motor driven electric vehicle with dynamic vibration absorbing structures," *J. Sound Vibrat.*, vol. 419, pp. 249–267, Apr. 2018.
[13] Y. Mao, S. Zuo, and J. Cao, "Effects of rotor position error on longitudinal vibration of electric wheel system in in-wheel PMSM driven vehicle," *IEEE/ASME Trans. Mechatronics*, vol. 23, no. 3, pp. 1314–1325, Jun. 2018.
[14] Y. Li, B. Li, X. Xu, and X. Sun, "A nonlinear decoupling control approach using RBFNNI-based robust pole placement for a permanent magnet in-wheel motor," *IEEE Access*, vol. 6, pp. 1844–1854, 2018.
[15] B. Li, A. Goodarzi, A. Khajepour, S.-K. Chen, and B. Litkouhi, "An optimal torque distribution control strategy for four-independent wheel drive electric vehicles," *Vehicle Syst. Dyn.*, vol. 53, no. 8, pp. 1172–1189, Aug. 2015.
[16] Z. Wang, C. Qu, L. Zhang, X. Xue, and J. Wu, "Optimal component sizing of a four-wheel independently-actuated electric vehicle with a real-time torque distribution strategy," *IEEE Access*, vol. 6, pp. 49523–49536, 2018.
[17] J. Liao, Z. Chen, and B. Yao, "Performance-oriented coordinated adaptive robust control for four-wheel independently driven skid steer mobile robot," *IEEE Access*, vol. 5, pp. 19048–19057, 2017.
[18] L. Zhai, T. Sun, and J. Wang, "Electronic stability control based on motor driving and braking torque distribution for a four in-wheel motor drive electric vehicle," *IEEE Trans. Veh. Technol.*, vol. 65, no. 6, pp. 4726–4739, Jun. 2016.
[19] T. Kobayashi, E. Katsuyama, H. Sugiura, E. Ono, and M. Yamamoto, "Direct yaw moment control and power consumption of in-wheel motor vehicle in steady-state turning," *Vehicle Syst. Dyn.*, vol. 55, no. 1, pp. 104–120, Jan. 2017.
[20] L. Guo, P. Ge, and D. Sun, "Torque distribution algorithm for stability control of electric vehicle driven by four in-wheel motors under emergency conditions," *IEEE Access*, vol. 7, pp. 104737–104748, 2019.
[21] J.-S. Hu, Y. Wang, H. Fujimoto, and Y. Hori, "Robust yaw stability control for in-wheel motor electric vehicles," *IEEE/ASME Trans. Mechatronics*, vol. 22, no. 3, pp. 1360–1370, Jun. 2017.
[22] B. Ren, H. Chen, H. Zhao, and L. Yuan, "MPC-based yaw stability control in in-wheel-motored EV via active front steering and motor torque distribution," *Mechatronics*, vol. 38, pp. 103–114, Sep. 2016.
[23] J.-S. Hu, D. Yin, and Y. Hori, "Fault-tolerant traction control of electric vehicles," *Control Eng. Pract.*, vol. 19, no. 2, pp. 204–213, Feb. 2011.
[24] S. Kim and K. Huh, "Fault-tolerant braking control with integerated EMBs and regenerative in-wheel motors," *Int. J. Automot. Technol.*, vol. 17, no. 5, pp. 923–936, Oct. 2016.
[25] R. Wang and J. Wang, "Fault-tolerant control with active fault diagnosis for four-wheel independently driven electric ground vehicles," *IEEE Trans. Veh. Technol.*, vol. 60, no. 9, pp. 4276–4287, Nov. 2011.
[26] R. Wang and J. Wang, "Fault-tolerant control for electric ground vehicles with independently-actuated in-wheel motors," *J. Dyn. Syst., Meas., Control*, vol. 134, no. 2, Mar. 2012, Art. no. 021014.
[27] G. Zhang, H. Zhang, X. Huang, J. Wang, H. Yu, and R. Graaf, "Active fault-tolerant control for electric vehicles with independently driven rear in-wheel motors against certain actuator faults," *IEEE Trans. Control Syst. Technol.*, vol. 24, no. 5, pp. 1557–1572, Sep. 2016.
[28] Y. Liao, "Analysis of fault conditions in permanent-magnet in-wheel motors," M.S. thesis, KTH Roy. Inst. Technol., Stockholm, Sweden, 2011.
[29] Y. Si, Y. Wang, and D. Zhou, "Key-Performance-Indicator-Related process monitoring based on improved kernel partial least squares," *IEEE Trans. Ind. Electron.*, early access, Feb. 13, 2020, doi: 10.1109/TIE.2020.2972472.
[30] Y. Wang, Y. Si, B. Huang, and Z. Lou, "Survey on the theoretical research and engineering applications of multivariate statistics process monitoring algorithms: 2008–2017," *Can. J. Chem. Eng.*, vol. 96, no. 10, pp. 2073–2085, Oct. 2018.
[31] Z. Zhou, M. Zhong, and Y. Wang, "Fault diagnosis observer and fault-tolerant control design for unmanned surface vehicles in network environments," *IEEE Access*, vol. 7, pp. 173694–173702, 2019.
[32] A. G. Jack, B. C. Mecrow, and J. A. Haylock, "A comparative study of permanent magnet and switched reluctance motors for high-performance fault-tolerant applications," *IEEE Trans. Ind. Appl.*, vol. 32, no. 4, pp. 889–895, Jul. 1996.
[33] N. Bianchi, S. Bolognani, and M. Dai Pre, "Strategies for the fault-tolerant current control of a five-phase permanent-magnet motor," *IEEE Trans. Ind. Appl.*, vol. 43, no. 4, pp. 960–970, Jul. 2007.
[34] J. A. Rosero, L. Romeral, J. A. Ortega, and E. Rosero, "Short-circuit detection by means of empirical mode decomposition and Wigner–Ville distribution for PMSM running under dynamic condition," *IEEE Trans. Ind. Electron.*, vol. 56, no. 11, pp. 4534–4547, Nov. 2009.
[35] O. Wallmark, L. Harnefors, and O. Carlson, "Control algorithms for a fault-tolerant PMSM drive," *IEEE Trans. Ind. Electron.*, vol. 54, no. 4, pp. 1973–1980, Aug. 2007.
[36] Y. Jeong, S.-K. Sul, S. E. Schulz, and N. R. Patel, "Fault detection and fault-tolerant control of interior permanent-magnet motor drive system for electric vehicle," *IEEE Trans. Ind. Appl.*, vol. 41, no. 1, pp. 46–51, Jan. 2005.
[37] R. Rajamani, *Vehicle Dynamics and Control*. New York, NY, USA: Springer, 2012.
[38] H. B. Pacejka, *Tire and Vehicle Dynamics*, 3rd ed. Amsterdam, The Netherlands: Elsevier, 2012.
[39] C.-Y. Lu and M.-C. Shih, "Application of the pacejka magic formula tyre model on a study of a hydraulic anti-lock braking system for a light motorcycle," *Vehicle Syst. Dyn.*, vol. 41, no. 6, pp. 431–448, Dec. 2004.
[40] Y.-J. Jang, M.-Y. Lee, I.-S. Suh, and K. Nam, "Lateral handling improvement with dynamic curvature control for an independent rear wheel drive EV," *World Electr. Vehicle J.*, vol. 7, no. 2, pp. 238–243, 2017.

KIBEOM LEE received the B.S. degree in mechanical and system design engineering from Hongik University, Seoul, South Korea, in 2012, and the M.S. and Ph.D. degrees from the Graduate School of Green Transportation, Korea Advanced Institute of Science and Technology (KAIST), Daejeon, South Korea, in 2014 and 2020, respectively. He is currently an Assistant Professor with the School of Mechanical Automobile Engineering, Halla University, and the Director of the Autonomous System Laboratory. His research interests include the fields of autonomous systems, vehicle dynamics and control, advanced driver assist systems, and autonomous vehicles.

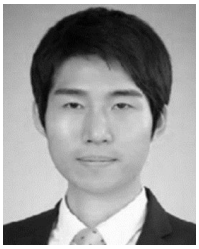

MINYOUNG LEE received the B.S. and M.S. degrees in mechanical and system design engineering from Hongik University, Seoul, South Korea, in 2010 and 2012, respectively, and the Ph.D. degree from the Graduate School of Green Transportation, Korea Advanced Institute of Science and Technology (KAIST), Daejeon, South Korea, in 2017. He was a Researcher with the Mechanical Engineering Research Institute and the Graduate School of Green Transportation, KAIST, from 2017 to 2018. He is currently a Senior Researcher with the Department of Smart Industrial Machine Technologies, Korea Institute of Machinery and Materials. His research interests include the robotic system control, sensor fusion, and computer vision.